

Accelerated Hit Series Identification with Target Evaluation, Deep Learning and Automated Labs: Prospective Validation in IRAK1

Gintautas Kamuntavičius¹, Alvaro Prat¹, Tanya Paquet¹, Orestis Bastas¹, Hisham Abdel Aty¹, Quing Sun², Marc Siladi², Dan Rines^{2*}, Sarah J. L. Flatters¹, Roy Tal¹, Povilas Norvaišas^{1*}

¹AI Chemistry, Ro5, 2801 Gateway Drive, Irving, 75063, TX, USA.

²Strateos, 3565 Haven Ave Suite 3, Menlo Park, 94025, CA, USA.

*Corresponding author(s). E-mail(s): dan.rines@strateos.com; pnorvaisas@ro5.ai;

Contributing authors: gkamuntavicius@ro5.ai; aprat@ro5.ai; tpaquet@ro5.ai; obastas@ro5.ai; habeldel-aty@ro5.ai; qing.sun@strateos.com; marc.siladi@strateos.com; sflatters@ro5.ai; rtal@ro5.ai;

Abstract

In this study, we integrate Ro5's target evaluation *SpectraView* and DL-driven virtual screening *HydraScreen* tools alongside Strateos' robotic cloud labs high-throughput screening platform to accelerate target and hit identification. Using SpectraView to select IRAK1 as the target, we prospectively validate HydraScreen, a structure-based deep learning model. We demonstrate that HydraScreen could identify up to 23.8% of all IRAK1 hits in the top 1% of the ranked compounds, simultaneously identifying the three most potent (nanomolar) scaffolds present in the library. The three nanomolar scaffolds identified in our project are novel for IRAK1 and lend themselves for future development. HydraScreen outperforms traditional virtual screening methods in an unbiased prospective evaluation and offers advanced features such as ligand pose confidence scoring. Thus, SpectraView and HydraScreen are innovative tools which can aid and expedite early stages of drug discovery.

Keywords: Artificial intelligence, machine learning, deep learning, drug discovery, SBDD, high-throughput screening, automated labs, IRAK1, interleukin 1 receptor associated kinase

1 Introduction

Drug discovery is a notoriously lengthy, expensive and inefficient process [10]. Many of its major challenges and bottlenecks are now being tackled by transforming the pharmaceutical industry's legacy workflows [38] using modern data management [48], lab automation [34, 33] and machine learning (ML) [35, 42, 6] solutions. Target identification and hit identification in early drug discovery provide perfect examples of such transformation [38]. Traditionally, target identification has always been a manual process driven by specialized domain-knowledge [23]. New data management and analysis systems have now augmented researchers workflows and allow them to easily integrate, summarize and search biomedical data for hypothesis generation. Examples of such systems include knowledge graphs [47] and target identification and evaluation platforms [5]. Similarly, the high-throughput screening (HTS) methods for hit identification rely on slow and costly unguided experimentation [50, 49]. The recently emerged automated robotic labs can now provide highly-reproducible data at greater throughput volume with better control of the experimental conditions [1, 16, 33].

Virtual screening for hit identification is one of the areas where machine learning (ML) and deep learning (DL) techniques can now offer previously unavailable solutions or better performance than the traditional alternatives [29]. Computational chemistry techniques such as docking [24], and quantitative structure-activity relationship (QSAR) models [12] are either being augmented (e.g. DL-based docking [28], Diffdock [9], DL force fields [41]) or complemented (e.g. CrossDocked CNN model [13]) with these methods. Many different ML-based protein-ligand interaction prediction methods are now available for application in virtual screening [29]. These methods are often extensively benchmarked and compared (e.g. K_{deep} [21]) using retrospective publicly available data. However, their translation to practice is still limited with only few prospective validation studies available [30], especially in comparison to the widely used computational chemistry techniques like docking [49]. The impact of these methods in the real-world drug discovery programs will ultimately depend not only on their raw performance, as tested in benchmarking studies, but also on their ability to prioritize targets and compounds that could be brought to later stages of drug development.

In this study, we demonstrate an early drug discovery workflow, which integrates Ro5's target evaluation (*SpectraView*) and DL-driven virtual screening (*HydraScreen*) [3] tools alongside Strateos robotic cloud labs for high-throughput screening. We perform data-driven target evaluation and prospectively validate Ro5's structure-based deep learning model HydraScreen in virtual screening. Using the HTS results collected by the robotic cloud labs we also benchmark HydraScreen against traditional techniques, such as molecular docking, Random Forest (RF) model, and shape-based methods. Finally, we evaluate the identified hits in terms of their potential for further development.

2 Methods

2.1 Target Evaluation using SpectraView

Target selection and evaluation was performed using Ro5's proprietary target evaluation tool *SpectraView*. This tool allows data driven evaluation of prospective protein targets in drug discovery projects by drawing relevant contextual information from Ro5's Knowledge Graph. The evaluation criteria encompass both scientific (e.g. biological, chemical) and business (e.g. novelty, competition) considerations. The evaluation follows criteria commonly encountered in the drug discovery projects that are presented as questions raised by the researchers. Results from these queries are presented as interactive visualizations that allow exploration of different criteria for thorough target evaluation.

Ro5's Knowledge Graph consists of 4 main components:

- ontologies - databases of entities with unique identifiers (e.g. Ensemble, HGNC),
- unstructured (textual) data - > 34M PubMed abstracts and >90M patents from which entities and their relationships are extracted
- structured (database) data - relational databases with contextual information for each entity type (20+ databases, 8 entity types, >2M annotated compounds, >1Bn compound library, >500k annotated gene/protein targets, >300k 3D structures, >20k diseases, >15M assay results, >250k clinical trials)
- metadata and metrics - data origin metadata and custom metrics for data science analytics.

As such, the Ro5's Knowledge Graph presents a comprehensive data resource for target evaluation.

The Knowledge Graph contains 12 entity types (Disease, Target, Mechanism, Compound, Species, Anatomical location, Cell line, Biomarker, Publication, Patent/Application, Author, Organization). Entity-to-entity edges are extracted for all of these entity pairs. Additionally, full contextual information is preserved when processing textual information by introducing a Publication entity. As a result, conditional queries can be formulated for all combinations of extracted entities (e.g. Target - Diseases in the context of a Mechanism in a given publication). For all of the textual information, extensive metadata is preserved, including journal, author and affiliation information. This information is then used to enrich the Knowledge Graph with the corresponding entities (e.g. Author, Organization) which can be used business-oriented analyses. Finally, the Knowledge Graph is populated with metrics that allow quantitative evaluation of the graph structure and entity dynamics (e.g. network connectivity, edge emergence, point-wise mutual information, etc.). Altogether, such detailed representation of entities and their relationships present in the biomedical literature and patents allow an in-depth and up to date analysis of various scientific queries for the drug discovery purposes.

2.2 Strateos Cloud Lab

All of the *in vitro* experiments were performed at the Strateos Cloud Lab. The Strateos Cloud Lab comprises a collection of online software applications that integrate Strateos' automated chemistry and biology workstations, inventory management, data generation and data management. All experiments are coded in autoprotocol, an open-source standard developed by Strateos (www.autoprotocol.org), which coordinates instrument actions in specific work cells based on scientific intent. This platform allows scientists to configure experiments and experimental parameters, remotely initiate and monitor automated experiments, oversee protocol management and inventory, generate data, and access real-time outputs of experimental data in a closed loop fashion.

2.3 47k diversity library

A diverse library of 46743 compounds was employed as the primary screening resource. This compilation, chosen from a broader pool of 500,000 compounds through cheminformatics evaluation, with properties like scaffold diversity, good chemical quality, and favorable physicochemical attributes. Compounds prone to interference were systematically removed, aligning with the exclusion of Pan Assay Interference Compounds (PAINS) from screening libraries. Compounds stocks were stored at 10mM in DMSO. For screening compounds were arrayed 50 μ l/well in Echo-qualified 384 well polypropylene microplates at room temperature for frequent use.

2.4 Strateos library ligand preparation & stereoisomer treatment

Strateos library compound SMILES were sanitized by removing salts and converting them into a canonical form. Stereoisomers of the same compound were treated as different ligands. For compounds with ≤ 4 unidentified stereocenters, all possible stereoisomers (up to 16) were generated and stored for further evaluation. Many compounds had more than > 4 unidentified stereocenters, leading to an exponential increase in the number of stereoisomers (e.g. triterpenoids with > 10 unidentified stereocenters). For these compounds we have selected a random subset of 16 stereoisomers that were used in virtual screening. This enumeration of stereoisomers has increased the number of compounds to be considered from 46743 to 65546. The results for all *in silico* methods were collected for all of the stereoisomers. A final per-compound score was calculated by computing the mean value of the scores of the stereoisomers.

2.5 HydraScreen

HydraScreen is machine learning scoring function (MLSF) composed of a CNN-based deep learning framework designed for accurate prediction of protein-ligand affinity and pose scoring [3]. For a given target protein, HydraScreen estimates the affinity of a query ligand in a twofold process. First, a set of protein-ligand conformations are generated, creating a docked pose ensemble. Second, the affinity and pose estimation of each conformation is estimated, and a final aggregate affinity value is computed

by means of a Boltzmann-like average of the protein-ligand conformational space. A schematic of the described procedure can be observed in Figure 1.

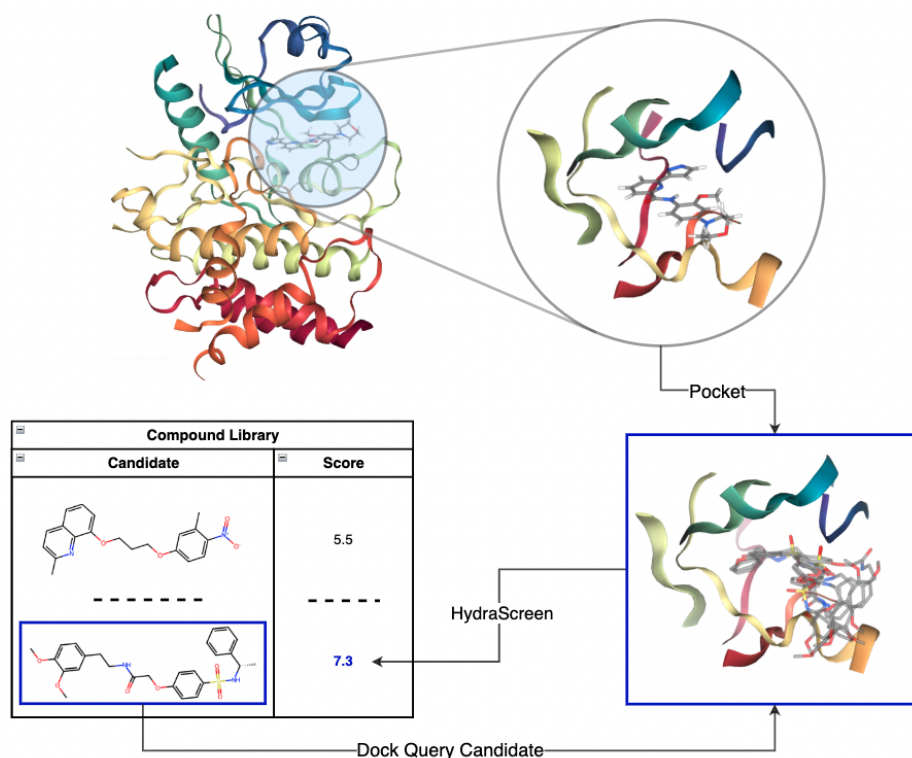


Fig. 1: End-to-end structure-based scoring via HydraScreen. interleukin 1 receptor associated kinase 1 (IRAK1) crystal structure 6BFN and the associated ligand DL1 were used to define the pocket and relevant residues (top). For each compound in the library a pose ensemble was created via docking. The pose ensembles were then used as an input in HydraScreen to predict the compound affinity and pose confidence scores.

Docked poses are generated in a similar fashion to that outlined in [3]. Briefly, we use the open-source Smina software, a fork of the AutoDock Vina software with a number of improvements, to generate poses of a query ligand in the pocket of our target protein. For each protein-ligand pair, the docking process involves: (1) preparation of the protein structure, (2) preparation of the ligand structure, and (3) docking with Smina. For the protein, the following steps were taken to prepare it for docking: (1) solvent and ion deletion, (2) repair of truncated side-chains using Dunbrack 2010 rotamer library [37], (3) adding hydrogens (histidines were treated like other standard residues), (4) adding charges. Non-standard residues were changed to the nearest standard residue. For example, selenomethionine (MSE) → methionine (MET). For

ligands, each ligand is sanitized through RDKit (2021.09.03), with hydrogens added prior to sanitization if the protonation state was incomplete or corrupt. We generate up to 20 poses per ligand query, and set the following Smina input parameters: (`num_modes`, 20), (`min_rmsd`, 1Å). Furthermore, we define the pocket by using the `autobox` option, passing in the reference crystal ligand pose (DL1) from 6BFN, and including all atoms within 4 Å of any atom in the native conformation.

In this study, we primarily use HydraScreen to find potential hits amongst a large compound library, therefore we rely on its ranking to identify compounds that successfully bind to the pocket above a given affinity threshold.

2.6 Benchmarks

We introduce a set of baselines for structure-based and ligand-based methods to better understand the contribution of HydraScreen with respect to traditional approaches.

Smina

In contrast to ranking our compounds according to our MLSF, Smina exploits a traditional structure-based approach. Herein, protein-ligand binding can be scored according to the energy required to remove a ligand pose from the pocket (free energy). In order to score our compounds, we leverage our already generated poses and, for each docked ensemble, extract the largest free energy calculated by Smina (amongst all the poses).

DeCAF

Density-Encoded Canonically Aligned Fingerprint (*DeCAF*) [39] is a ligand-based approach that measures the similarity between two molecules. *DeCAF* can be used to rank compounds by rewarding similarity between the query candidate and the reference molecule (DL1). *DeCAF* score is computed by: (i) Finding the maximal common subgraph between the corresponding molecular graphs, represented as a coarse network of pharmacophore descriptors; (ii) Computing the modular product of the two graphical models and extracting the similarity between the maximal clique identified. In contrast to other shape-based methods like *USRCAT* [36], DeCAF does not require conformer generation.

Random Forest

We have trained a Random Forest (RF) classifier using publicly available IRAK1 data. We convert the available pKi and pIC₅₀ values for IRAK1 to boolean values based on whether they are over or under the micromolar range > 6 pIC₅₀ threshold. Out of 689 molecules available on PubChem, 142 were active and 547 were inactive. The inactive class was further up-sampled by 5K by using DeepCoy [20]. The compounds generated with DeepCoy were ensured to be structurally dissimilar to the actives while maintaining similar molecular weight as well as synthetic accessibility. The classified model was trained using ECFP4 fingerprints [31] generated using RDKit.

Pharmit

Pharmit [40] provides an online, interactive environment for the virtual screening of large compound databases using pharmacophores, molecular shape and energy minimization. Queries are specified in terms of a pharmacophore, a spatial arrangement of the essential features of an interaction, and molecular shape. Search results can be further ranked and filtered using energy minimization. Pharmit uses state-of-the-art sub-linear algorithms to provide interactive screening of millions of compounds. Queries typically take a few seconds to a few minutes depending on their complexity.

We used the co-crystallized structure 6BFN to extract a 6-point pharmacophore hypothesis, later used in scoring the HTS compounds. In order to create a continuous score that can be used to rank the compounds rather than a boolean match, we extended Pharmit's compound and hypothesis matching functionality. The continuous score was computed by evaluating subsets of the original pharmacophore hypothesis, performing conformer matching on them and then combining results from the subset matches to get the final score. Such a hypothesis-subset screening was made possible by the highly efficient nature of the Pharmit algorithm.

2.7 IRAK1 assay

Purified recombinant IRAK1-His (cat. # 40202) was purchased from BPS Bioscience Inc. (San Diego, CA, USA). Kinase tracer 236 (cat. # PR9078A) was purchased from Thermo Fisher Scientific Inc. (Waltham, MA, USA) Eu-W1024-anti-6xHis antibody (cat. #AD0400) and 384-well white ProxiPlates™ (cat. # 6008289) were purchased from Perkin Elmer, Inc. (Waltham, MA, USA). Echo-qualified 384 well COC low dead volume source microplates (cat. #001-16128) and Echo-qualified 384 well polypropylene microplates (cat. #001-14615) were purchased from Beckman Coulter Inc. (Indianapolis, IN, USA).

LanthaScreen™ Eu Kinase Binding Assay for IRAK1 The experimental method was developed based on the Invitrogen™ IRAK1-GST LanthaScreen™ binding assay. The assay was carried out in an enclosed workcell with subdued lighting. All reagents were prepared in the assay buffer (50 mM HEPES, 10 mM MgCl₂, 1 mM EGTA, 0.01% Brij-35, 1 mM DTT) and kept on ice. These included 2 x tracer 236 (0.2 μM), 2 x IRAK1 /antibody solution (20 nM IRAK1-His, 4 nM Eu-W1024-anti-6xHis antibody) and 2 x antibody solution (4 nM Eu-W1024-anti-6xHis antibody). Five microliters of 2 x tracer 236 was dispensed into a 384-well white ProxiPlate™, followed by either 5 μl of 2 x IRAK1/antibody solution or 5 μl of 2 x antibody solution on a Tempest® dispenser (Formulatrix, Inc., Bedford, MA, USA). The plate was sealed on a Wasp plate sealer (KBiosciences Limited, Basildon, Essex, UK) and centrifuged at 1000 x g for 15 seconds on a HiG™ automated centrifuge (BioNex Solutions Inc., San Jose, CA, USA) and incubated at room temperature for 30 minutes. The plate was then peeled and read on a PHERAstar® FSX (BMG LABTECH Inc., Cary, NC, USA) with a LanthaScreen™ module at 340/615, 665 nm. The TR-FRET ratio (acceptor emission/donor emission x 10000) was used as the readout.

Biovalidation and pilot screen

Biovalidation was carried out with identical assay settings as for the anticipated production runs. Assay conditions and the instrument settings were tested for their performance within the acceptance criteria ($Z' \geq 0.5$ (see eq. 1, where p and n refer to positive and negative control wells in the plates), no visible patterns on assay plates). Compounds from 2 library plates were dispensed at 10 nL/well in single point in columns 3 to 22 on assay plates (final concentration in assay at 10 μ M) and 10 nL/well of DMSO was dispensed in columns 1, 2, 23 and 24 for controls. Ten nanoliter per well of DMSO was dispensed into all wells on positive and negative control plates. Compounds and DMSO were dispensed on an Echo 655 liquid handler in an Access workstation. For the kinase binding assay, the 2 x tracer solution was dispensed into all wells on all plates. For the assay plates, the 2 x IRAK1/antibody solution was dispensed into columns 1 and 3 to 23. The negative control plates have the same layout as the assay plates, with DMSO in place of the compounds. For the positive control plates, the 2 x antibody solution was used in place of the 2 x IRAK1/antibody solution in columns 3 to 22. Six plates were dispensed in total, including 2 assay plates, 2 negative control plates and 2 positive control plates. The compound dispense run and the binding assay run were both set up and launched in the Cloud Lab. The automated runs were carried out in the workcells and with the autoprotocols designated for production. Z' , signal-to-background ratio and compound hit rate were analyzed as performance parameters.

$$Z' = 1 - \frac{3(\sigma_p + \sigma_n)}{|\mu_p - \mu_n|} \quad (1)$$

Biovalidation was followed by a pilot screen with a plate number close to that in a production run for evaluation of the robustness of the assay, the automation scheduling and the data transfer. Compounds from 20 library plates were dispensed onto 20 assay plates. Two positive and two negative control plates were used in the same manner as in biovalidation. The screen was carried out with the same lot of reagents, procedure, instrument settings and autoprotocols as in biovalidation. Z' , signal-to-background ratio and compound hit rate were analyzed as performance parameters.

2.8 High-throughput screen (HTS)

Primary screen

The primary screen runs were performed with the same reagents and procedures as the pilot screen. Up to 40 plates were assayed per run. In total 153 plates and 46743 compounds were screened at 10 μ M in single point. Plate quality control was performed using manual inspection and Z' analysis (equation 1). Plates not passing with $Z' \geq 0.5$ were run repeatedly.

Primary screen data analysis

With the collected fluorescence data we have performed per-plate fluorescence normalization. Normalization entailed using negative control (DMSO) and positive control (Staurosporine) to scale scaling the fluorescence in the ratio channel (see Equation

2). Mean values from the 32 negative control (μ_{DMSO}), and 32 positive control (μ_{SS} - Staurosporine) wells in each plate were used in the normalization.

$$ratio_{norm} = \frac{ratio_{raw} - \mu_{DMSO}}{\mu_{SS} - \mu_{DMSO}} \quad (2)$$

After the normalization the values in the fluorescence ratio channel represented the relative inhibition of IRAK1. Here, 0% values corresponded to the negative control - no inhibition, and 100% to the positive control - inhibition with staurosporine. The distribution of normalized fluorescence ratio values is presented in Figure 2. Only normalized fluorescence ratio channel values were used in further analysis. The threshold for hit selection was chosen to be 50% inhibition of IRAK1 relative to staurosporine. Using this threshold 353 hit compounds were identified.

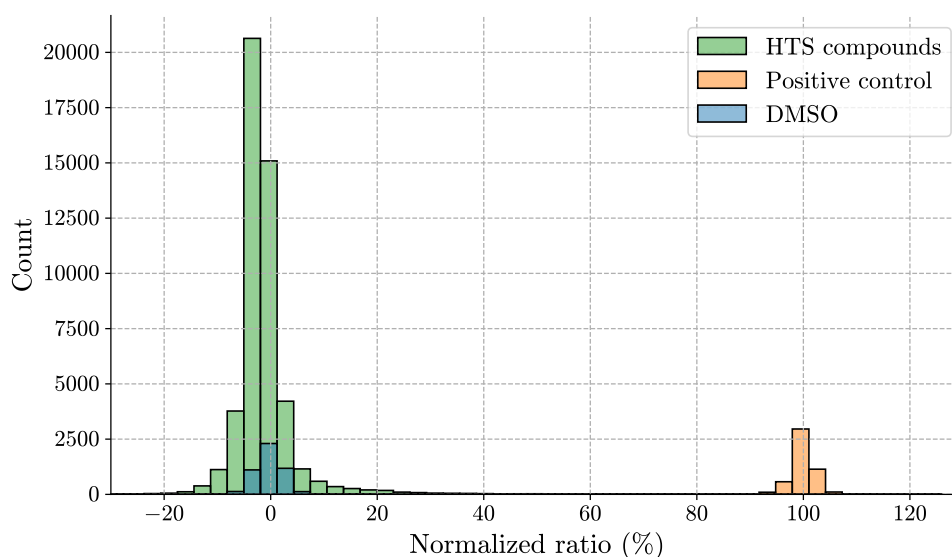


Fig. 2: Normalized fluorescence values in the ratio channel from the IRAK1 HTS. Values from the individual compounds from the library, positive and negative control wells are represented in different colors. Here 0% corresponds to the mean normalized fluorescence ratio in negative control wells and 100% to normalized fluorescence ratio in positive control wells across the whole library. Positive control represents IRAK1 inhibition with staurosporine.

Single-dose hit confirmation

For single-dose hit confirmation we have selected the 10 plates with the most hits and assayed them at 10 μM in duplication. The experiments showed high consistency with Z' values above 0.6 in all plates and high correlation between the replicates.

Compound clustering

The 353 hits identified via HTS were subsequently clustered by their structural similarity using the Louvain algorithm [4]. The algorithm identifies clusters ("communities") within a graph of related compounds that is constructed using compound Tanimoto similarity (TS) based on compound Morgan fingerprints. The Louvain algorithm was chosen for its compatibility with Tanimoto similarity and robustness in terms of the number of clusters in the dataset. In total, 200 unique clusters were identified, 160 of which were singletons. 5 compounds with the greatest ligand efficiency (LE) values were selected from each cluster to form a diversified set of 283 hits.

Hit dose-response assay

A dose response assay was performed for each of the diversified set of 283 hit compounds. Each compound was assayed in an 8-point curve with an approximately 4-fold (subject to Echo dispense volume limits) dilution starting at 30 μM in triplicates. The exact concentrations are 30, 7.5, 1.875, 0.469, 0.117, 0.029, 0.007, 0.002 μM . On each plate, three replicates of a staurosporine titration curve starting at 3 μM were assayed in parallel as the reference.

Hit dose-response data analysis

The IC_{50} of each dose-response curve was derived by fitting a four-parameter logistic (4PL) model, shown in Equation 3. The variables of the model are shown in Equation 3:

- *A*: Minimum asymptote. It's the response value when x approaches infinity.
- *D*: Maximum asymptote. It's the response value when x is very small or close to zero.
- *B*: Slope factor or Hill's slope. It describes the steepness of the curve.
- *C*: Inflection point. The concentration of the analyte that gives half-maximal response.

$$f(x) = A + \frac{D - A}{1 + \left(\frac{x}{C}\right)^B} \quad (3)$$

The 4PL model was fitted for each compound with data points for all three replicates all at once. The resulting in a pIC_{50} distribution as seen in Figure 3. As an additional quality control, fits for all submicromolar compounds were manually inspected. In 7 cases the model fits were erroneous and the IC_{50} values were reduced to 30 μM , the highest concentration of the assay. Whenever the model produced fits with IC_{50} values higher than 30 μM , the largest measured concentration in the assay, the IC_{50} values were made to be equal to 30 μM , or equivalently, $\sim 4.52 \text{ pIC}_{50}$.

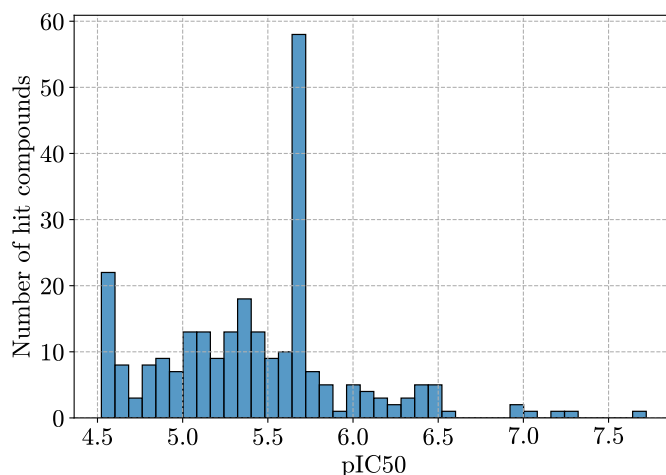


Fig. 3: Distribution of $-\log_{10}$ -normalized IC_{50} values (pIC_{50}) for the 283 hit compounds for which the dose-response data was collected.

3 Results

3.1 Target evaluation using SpectraView

3.1.1 Target evaluation goals and criteria

Multiple protein targets were considered for the joint Ro5-Strateos project. The targets were proposed by Strateos based on the availability of scalable assays and interest from their potential customers. In order to perform a thorough assessment of each target, we employed Ro5's target evaluation tool: SpectraView. Our aim was to identify a therapeutically relevant and commercially viable target for a drug discovery project, which could also be used for the prospective validation of Ro5's HydraScreen model. SpectraView relies on Ro5's integrated Knowledge Graph to serve information from multiple data sources (see methods section 2.1) following these queries:

- Availability of a crystal structure
- Existing biochemical data
- Existing drugs and most potent compounds
- Publication count and trends
- Novelty/Traction balance
- Target-disease associations
- Translation from academia to industry
- Competitive landscape

One of the main considerations when selecting a target in drug discovery is its novelty/confidence trade-off [23]. Most of the targets considered for the project were very well-studied, as marked by the volume of PubMed publications mentioning them (e.g. 800 articles mentioning KDR were published each year, see Appendix Fig. A1),

Table 1: Targets considered for the Ro5-Strateos project and some of the data used in target evaluation. Data from RSCB PDB [25], PubChem [22] and DrugBank [46] as of start of the project on 2022-01.

Target	Crystal structures, n	Data points, thousands	Max affinity, nM	FDA approved drugs, n
JAK1	44	6.5	< 0.01	5
JAK2	115	10.0	< 0.01	5
JAK3	38	6.0	< 0.001	5
TYK2	38	3.5	< 0.7	1
IRAK1	1	1.3	< 5.6	0 / 1 inv. ^a
FGFR1	59	7.0	0.2	5
FGFR2	37	2.1	0.1	7
FGFR3	4	4.5	0.1	9
FGFR4	28	2.0	0.1	6
RIPK2	24	0.2	1.3	0 / 1 inv.
VGFR2 (KDR)	45	18.0	0.02	2
TAK1 (MAP3K7)	19	0.3	1	-

^a Early clinical studies of IRAK1 inhibitor R835 [26].

availability of crystal structures, biochemical assay data and approved or investigational drugs (Table 1). We have focused on the relatively less established targets with lower volume of publications, fewer data points and only few known high activity compounds - IRAK1, FGFR3 and TAK1.

The availability of a crystal structure and biochemical assay data were crucial criteria when selecting a target for virtual screening and subsequently the prospective validation of HydraScreen. The crystal structure is necessary to generate poses between the ligand and binding site for predictions by HydraScreen and docking, while public assay data would be used in *DeCAF* pharmacophore-based comparison and for building ligand-based QSAR models. All of the considered targets had at least 1 crystal structure (Table 1). IRAK1, one of the least established targets, had a recent publication with its crystal structure resolved [43] (6BFN) and 1.3k biochemical assay data points. Moreover, IRAK1 was not present in HydraScreen’s training data set, allowing the method’s unbiased and fair prospective validation. IRAK1 thus satisfied the minimal requirements for selection, while also being the most underexplored target in the selection.

Additional evidence was needed to substantiate IRAK1’s choice for a drug discovery program in terms of its therapeutic links. In contrast to many other kinases, IRAK1 is primarily associated with inflammation (Fig. 4, e.g. [18]) and not cancers. It’s only recently that IRAK1 has been implicated in multiple cancers, including breast cancer [44], lymphoma [14] and acute myeloid leukemia [17]. The combination of fewer publications and emerging new therapeutic links provides additional support for IRAK1’s selection.

Finally, IRAK1 was assessed in terms of the potential competitors in the drug development effort. We have analyzed the competitive landscape by querying the publications and patents held by major pharma companies as well as the most potent drugs

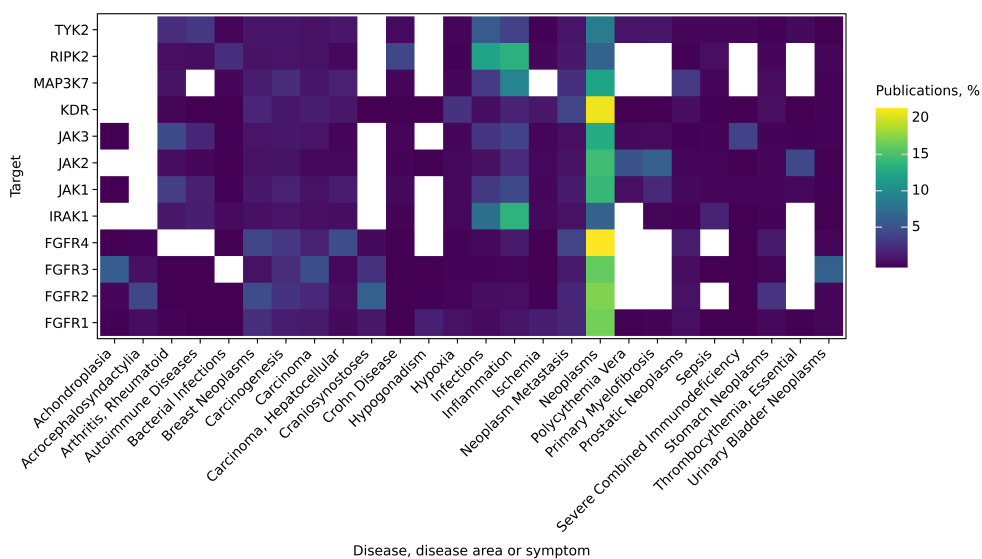


Fig. 4: Diseases, disease areas and symptoms co-mentioned with each of the considered targets. Colors represent the fraction of PubMed-indexed publications per disease for each of the targets.

and compounds reported in the public domain. We have found only few PubMed-indexed publications with affiliations linked to major pharma companies: Johnson and Johnson - 4, Genentech - 2, Roche - 2, GlaxoSmithKline - 2, Pfizer - 2, Novartis - 1, Rigel - 2 (Fig. A3). This was a promising finding, given much greater academic interest in IRAK1 with 637 publications (Fig. A5). Similarly, we have looked into patent and patent applications (Fig. A4). The majority of patents mentioning IRAK1 were owned by two academic institutions - Dana Farber Cancer Institute and Yisum Research and Development Company of the Hebrew University with both of these entities holding 14 patents each. No major pharmaceutical companies were found to hold patents linked to IRAK1. We have then looked into the most potent compounds active against IRAK1. Only few nanomolar compounds have been reported for IRAK1 (e.g. JH-X-119-01 is 9 nM, [14]). IRAK1 has been shown to be an off-target of an active metabolite R406 of FDA approved drug Fostamatinib developed by Rigel pharma for the treatment of chronic immune thrombocytopenia [32]. Rigel pharma has recently started pre-clinical and clinical studies of IRAK1/4 inhibitor R835 which has shown potential in murine models of multiple inflammatory diseases, including arthritis and lupus. However, has not yet received FDA approval [26]. The combination of largely academic research in IRAK1 with only recently emerging interest by pharmaceutical companies (Fig. A5), especially the supporting pre-clinical and clinical work [26, 32] provides corroborative evidence for its potential as a prospective drug target. The lack of any FDA-approved IRAK1 targeting drugs leaves an opportunity for the development of novel small molecule inhibitors. Altogether, the balance between the

novelty and sufficient support in terms of biochemical and biological rationale as well as competitive considerations made IRAK1 an attractive target to be pursued in this Ro5-Strateos study.

3.2 Identification of IRAK1 hits using HydraScreen

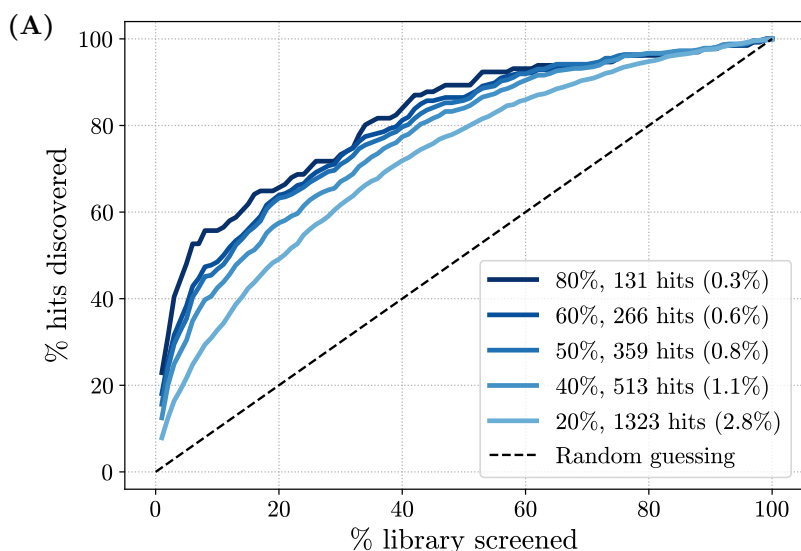
3.2.1 HydraScreen virtual screen

Following the selection of IRAK1 as a target using SpectraView, we performed *in silico* virtual screening for IRAK1, subsequently followed by experimental hit identification via HTS. The goal of this stage of the project was to perform prospective evaluation of HydraScreen's [3] performance using *in vitro* data collected by Strateos HTS in comparison to traditional, industry-standard methods like *Smina* [24] (molecular docking), *DeCAF* [39] (pharmacophore modeling) and a RF model trained on IRAK1 assay data that is publically available. Together, these results will provide a comprehensive and unbiased evaluation of HydraScreen as a virtual screening method.

In order to prospectively evaluate Ro5's HydraScreen model's performance in hit identification, we performed a virtual screen of the entire Strateos 47k compound diversity library (see Methods 2.5). HydraScreen predictions were then used to rank the library and select the top 1% (470) compounds to be considered *in silico* hits. Strateos subsequently performed an *in vitro* HTS with the same library (see Methods 2.8), which returned 353 hit compounds. These compounds were compared to the ones ranked in the top 1% by HydraScreen. In total, 57 compounds were discovered by HydraScreen that were also identified in the HTS, constituting a 15.9% hit discovery rate via virtual screening (see Supplementary Material).

Next we have investigated the impact that different IRAK1 activity thresholds for hit selection in HTS can have for hit identification in the HydraScreen virtual screen (Fig. 5). This is an important consideration, because both the virtual *in silico* and the high-throughput *in vitro* screens rely on arbitrary thresholds for hit selection [50, 49]. Here, we consider the comparison of virtual screening predictions against the HTS results for each individual compound in the ranking generated by HydraScreen. Virtual screening hit recovery rate for HydraScreen was estimated as a proportion of hits identified per number of compounds screened or tested. Standard HTS protocols randomly test compounds from the library (i.e. in the order in which they are stored); therefore, the hit recovery rate of traditional HTS is roughly proportional to the percentage of the library screened, as marked by the diagonal black line in Figure 5A. Any method that is able to prioritize active compounds over the inactive ones would provide a better hit recovery rate than random sampling (i.e. above the diagonal line in Fig. 5A).

We found that ranking the compound library according to HydraScreen predictions greatly increases hit discovery rates in virtual screening for IRAK1. This result is consistent for any number of top compounds selected in the ranking and any >0% threshold of relative IRAK1 inhibition in HTS. Using the 50% IRAK1 inhibition threshold, as was used in the *in vitro* experiment, HydraScreen identified 35.4% of the hit compounds within the top 5% and 63.7% with 20% of the ranking (Fig. 5B). Notably, close to 90% of the hits can be identified with only 50% of the ranking (see



(B)

Ratio (%)	Library screened (%)			
	1	5	20	50
80	23.8	48.4	66.7	90.5
60	18.5	38.5	64.6	86.9
50	15.9	35.4	63.7	86.1
40	12.6	30.4	57.8	84.2
20	7.7	21.5	49.1	79.3

Fig. 5: (A) HydraScreen hit discovery rate (% of hits discovered per library screened) for different IRAK1 inhibition thresholds in HTS (ratio %, marked by lines of in the shades of blue). For each IRAK1 inhibition threshold the number of hits identified in HTS is presented together with the overall HTS hit rate. Dashed black line represents random compound ranking. Supporting data is presented in table (B).

Figure 5B). Generally, HydraScreen exhibits better performance at higher IRAK1 assay inhibition thresholds. For example, HydraScreen identified 23.8% (30 out of 126) of hits at the top 1% of the compound ranking when using 80% relative inhibition threshold of IRAK1 (Fig. 5B).

The number of distinct highly active scaffolds identified in HTS can be more relevant than the total number of hits. Greater variety of scaffolds provides medicinal chemists with more opportunities for lead series development, which is crucial at the later stages of drug discovery [19]. Therefore, in addition to hit discovery rates, HydraScreen's performance was also assessed in terms of its ability to prioritize highly active compounds that are also structurally diverse. This would provide evidence

both for models ability to predict ligand potency, and lack of structural biases in the prioritization of the compounds.

To select a diverse, representative and unbiased set of compounds to screen in the secondary assay, the 353 hits from HTS were clustered by their structural similarity using the Louvain algorithm [4]. In total, 200 unique clusters were identified, 160 of which had single compound member. Scaffolds associated with each cluster were identified using maximum common substructure (MCS) analysis. Five compounds with the greatest ligand efficiency (LE) values were selected from each cluster to form a diversified set of 283 hits from 200 distinct scaffolds. For these 283 diversified hit compounds, Strateos collected dose-response data (see methods 2.8). Based on their pIC_{50} ($-\log_{10}$ transformed IC_{50}) activity values, hits and their corresponding scaffolds were grouped into micromolar, high nanomolar and nanomolar groups (Table 2). We identified 5 nanomolar and 25 high nanomolar hits, while the rest possessed micromolar activity (Fig. 6). Scaffolds were labeled based on the most active compound in each cluster. Out of the 200 total scaffolds, 15 were labeled as high nanomolar and 3 as nanomolar. We will refer to the union of high nanomolar and nanomolar compounds as *sub-micromolar*.

Table 2: Dose-response assay results for 283 diversified hits. Compounds and scaffolds were labeled as micromolar, high nanomolar and nanomolar based on the their pIC_{50} values. For scaffolds, the highest activity found in the correspond cluster of compounds was used as a label.

	pIC50 range	Compounds	Scaffolds
Micromolar	< 6	253	182
High nanomolar	$6 \leq x < 7$	25	15
Nanomolar	≥ 7	5	3

The dose-response data was used to evaluate HydraScreen’s performance in terms of discovery of highly active scaffolds (Fig. 7). We considered a scaffold to be ”discovered” by a model if at least one compound from the corresponding cluster was ranked by the model in top $X\%$ of the library. Notably, HydraScreen successfully recovered compounds belonging to all 3 nanomolar scaffolds within the top 1% of the library. Within the top-ranked 2%, HydraScreen recovered 8/18 of the submicromolar scaffolds. The remaining 10 scaffolds were present in the top 50% of the ranked compounds.

3.2.2 HydraScreen comparison against other virtual screening techniques

Virtual screening can be performed using a range of different techniques [27]. It is therefore relevant to evaluate HydraScreen’s performance in comparison to different traditional methods. In parallel to the HydraScreen virtual screen, we also prospectively generated predictions using *Smina* docking [24], *DeCAF* 2D pharmacophore matching [39], *Pharmit* 3D pharmacophore hypothesis matching [40] and a RF model

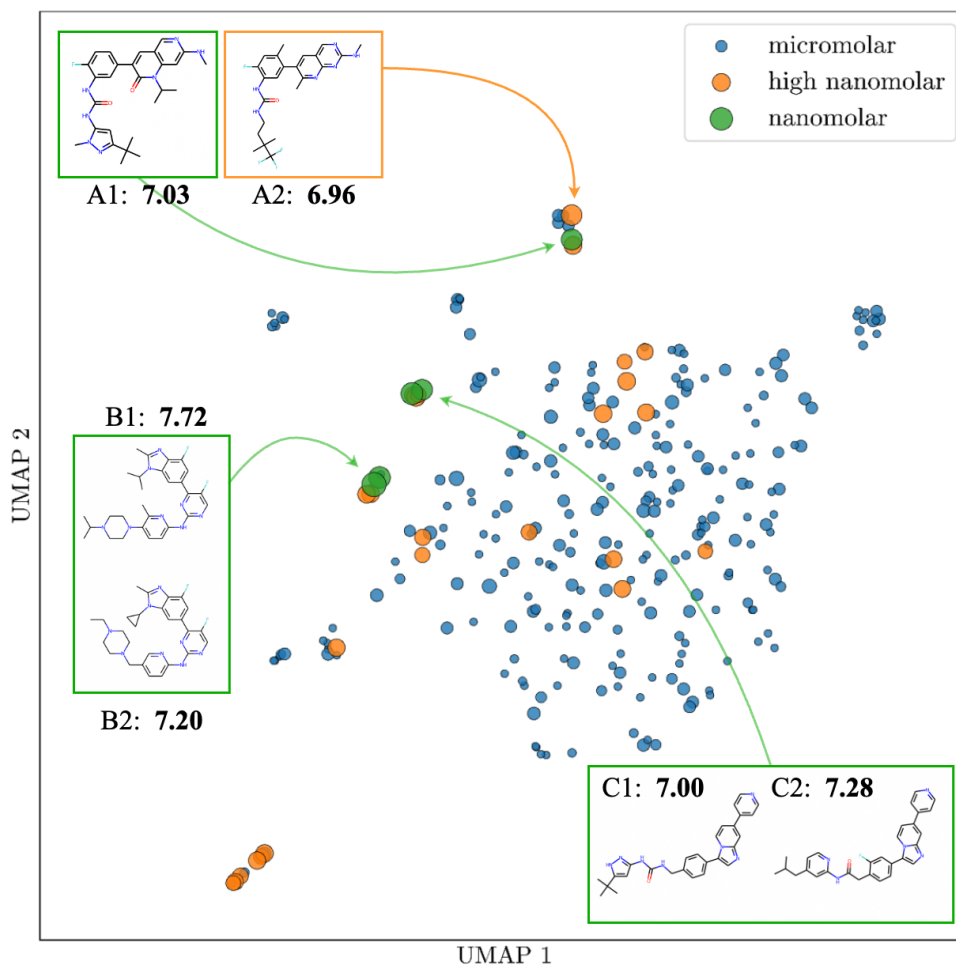


Fig. 6: UMAP embedding of 283 hit compounds from HTS screen. The space in the plot represents relative similarity of the compounds. Nanomolar compounds from the three nanomolar scaffolds are highlighted with their pIC_{50} values indicated underneath.

trained on ECFP4 fingerprints. The comparison between methods was made at the 50% IRAK1 inhibition threshold used in *in vitro* HTS, with 353 hits identified in total. HydraScreen considerably outperforms the traditional techniques and its hit identification rate is consistently higher for any selected percentage of the top ranked compounds. At the top 1% ranking the model provides 3.5x better performance than *Smina*, 3.2x better than RF with ECFP4 (Fig. 8B) and ~20 better performance than pharmacophore-based methods *Pharmit* and *DeCAF*. Both *Smina* docking and

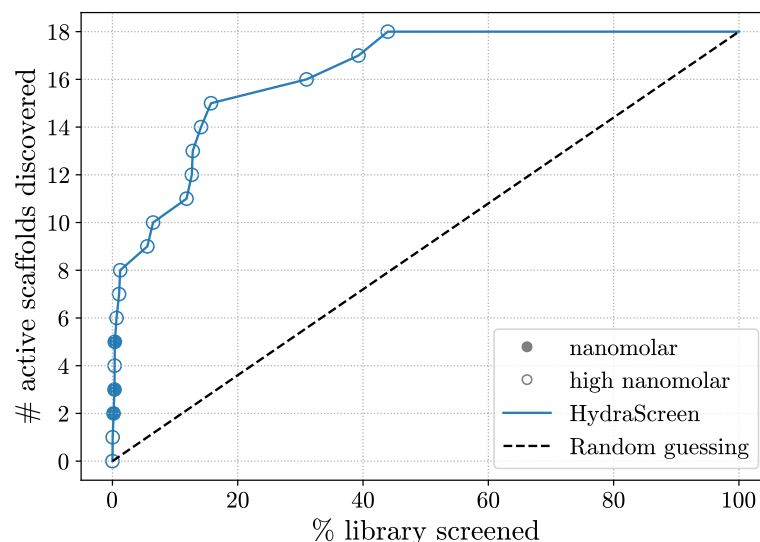


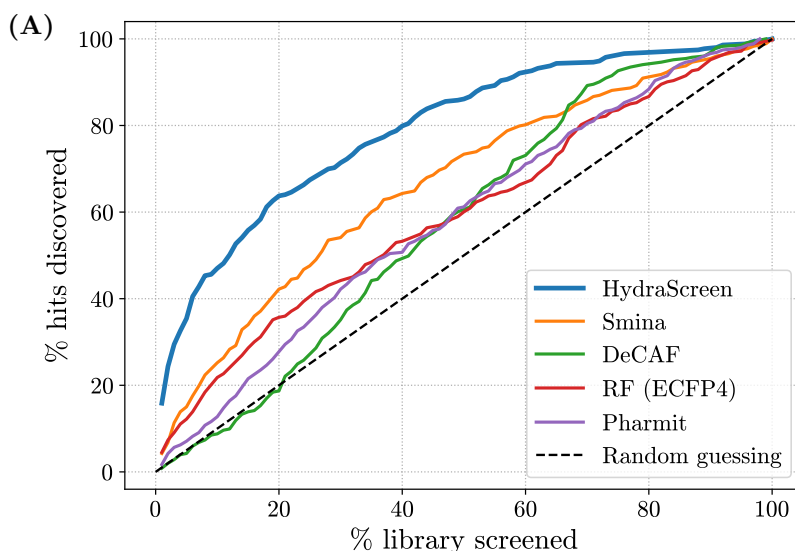
Fig. 7: HydraScreen distinct scaffold discovery rate (number of distinct scaffolds discovered per library screened). Dashed black line represents random compound ranking. Filled and empty circles represent nanomolar and high nanomolar scaffolds, respectively.

random forest perform similarly, and outperforming the pharmacophore based methods. However, for low ranked compounds (>70% ranking) *DeCAF* exhibits better performance than docking.

Following the same methodology used for evaluating HydraScreen in terms of its ability to rank distinct active scaffolds, we compared different virtual screening methods. As before, we considered a scaffold "discovered" if at least one compound from that scaffold was ranked in the corresponding library screening range. In comparison to other methods, HydraScreen exhibits superior scaffold discovery rates (Fig. 9A). Within the top 1% of the ranked compounds, HydraScreen discovered all three nanomolar and, in total, 6 out of 18 submicromolar scaffolds (Fig. 9B). In comparison, docking ranked the three nanomolar scaffolds only at 18% of the ranking, *Pharmit* at 27% and RF at 30%. Random forest ranked one of the nanomolar scaffolds in the top 10 compounds (0.02%). This scaffold is has a highly similar analogue in the public IRAK1 data that the RF model has trained on. This scaffold and the analogue are discussed in more detail in Section 3.3.1.

3.3 IRAK1 hits

IRAK1 hit identification via HTS experimentally discovered 283 hit compounds, representing 200 distinct structural scaffolds. In the last stage of the project, we evaluated these compounds and scaffolds in terms of their novelty, physio-chemical properties and IRAK1 binding modes.



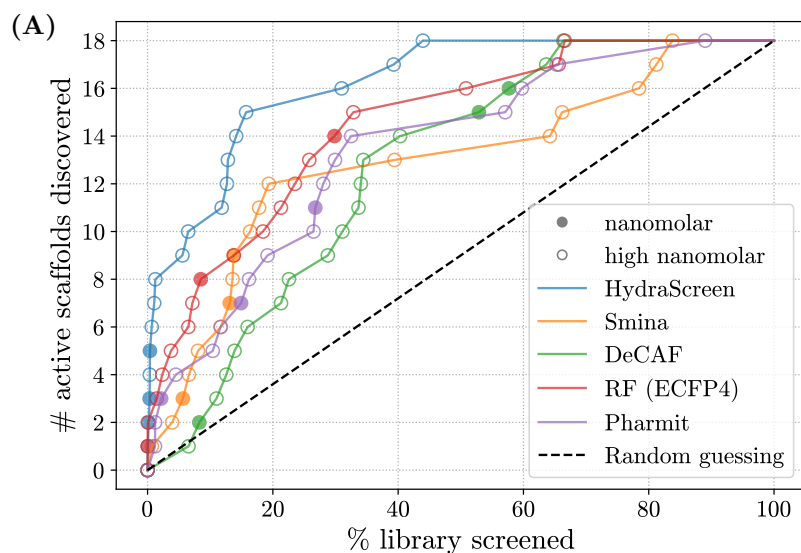
(B)

Method	Library screened (%)			
	1	5	20	50
HydraScreen	15.9	35.4	63.7	86.1
<i>Smina</i>	4.2	15.0	42.2	73.4
<i>DeCAF</i>	0.8	4.2	19.0	60.6
<i>Random Forest</i>	4.5	12.2	35.7	60.1
<i>Pharmit</i>	1.7	7.1	27.8	61.2

Fig. 8: (A) Hit discovery rates provided by different methods in IRAK1 virtual screen. Dashed black line corresponds to random compound ranking. Supporting data is presented in table (B).

3.3.1 Hit novelty and properties

In order to assess the uniqueness of the 283 diversified hits, we compared them against IRAK1 actives available in PubChem. Out of the 689 compounds reported to be active against IRAK1, 141 had sub-micromolar activity (>6 pIC₅₀). For each of the 283 hits, we found the nearest neighbor in the set of IRAK1 actives and scaffolds based on the Tanimoto Similarity (TS) between their Morgan fingerprints. The number of neighbors above a certain similarity threshold is reported in Table 3. We observe that the vast majority of compounds are distinct from publicly known actives, not having related chemical matter with a TS <0.4 in the public domain. Only 39 compounds, corresponding to 27 distinct scaffolds, exhibit >0.4 TS. Focusing on the nanomolar hit compounds, only 1 of the 3 scaffolds had a similar (TS <0.4) active compound in



(B)

Method	Library screened (%)			
	1	5	20	50
HydraScreen	5	8	15	18
<i>Smina</i>	1	2	12	13
<i>DeCAF</i>	0	0	6	14
<i>Random Forest</i>	2	5	10	15
<i>Pharmit</i>	1	4	9	14

Fig. 9: (A) Scaffold discovery rates provided by different methods in IRAK1 virtual screen. Nanomolar and high nanomolar scaffolds are marked by filled and empty circles correspondingly. Dashed black line corresponds to random compound ranking. Supporting data is presented in table (B).

the public domain; the closest structure was the Pan-RAF inhibitor LY3009120 [15] with a TS of 0.82. A whole cell-based kinase screen revealed that LY3009120 displayed some IRAK1 inhibition (390 nM IC_{50}), though it was not the primary target of the compound.

The 30 sub-micromolar hit compounds represented 18 distinct scaffolds, with the 6 most active compounds spanning 3 of these as indicated in Figure 6. The 6 most active compounds are synthetically tractable, with synthetic accessibility scores in a similar range to that of catalogue compounds (2-3) [11]. They border on the upper end of the Lipinski rule of 5 [8] with regards to molecular weight (466 to 521 g/mol) and Crippen LogP values of 4.7 to 6 [45]. The high molecular weight and LogP nature will have to be further assessed during a medicinal chemistry program.

TS threshold	Hits	Scaffolds	Nanomolar scaffolds
Total	283	200	3
> 0.4	21	13	1
> 0.6	5	3	1
> 0.8	1	1	1
> 0.9	0	0	0

Table 3: Numbers of hits and scaffolds that have at least one neighbor in the IRAK1 public dataset that is more similar than the specified Tanimoto similarity (TS) threshold.

3.3.2 HydraScreen hit compound binding modes

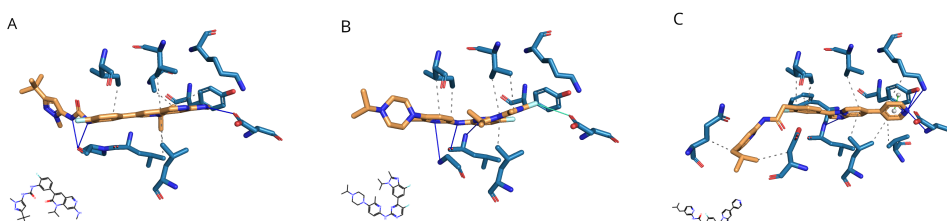


Fig. 10: IRAK1-ligand poses with the highest HydraScreen confidence for selected nanomolar hits A1, B1, and C2, represented in panels A, B, and C respectively. PLIP protein-ligand interactions are shown with grey dashes (hydrophobic interactions), blue lines (H-bonds), and green dashes connecting white spheres (pi-pi stacking).

In addition to ranking compounds according to their predicted affinity against a target, HydraScreen provides insight into the likely binding modes of the compounds by predicting pose confidence for the docked poses. To describe the HydraScreen predicted binding for the most active compound of each of the nanomolar scaffolds (compounds A1, B1, and C2 in Figure 6), the IRAK1-ligand interactions of the predicted highest confidence pose were identified using the protein-ligand interaction profiler, PLIP [2]. Across the highest confidence poses, the sequential aromatic heterocycles of the compounds were situated towards the back of the ATP binding pocket, with hydrophobic interactions with valine (V226), leucine (L347), and isoleucine (I218) residues (Fig. 10). The central heterocycles of compounds B1 and C2 forms hydrogen bonds (H-bonds) with the hinge region, whereas the urea in A1 forms H-bonds to the backbone. Both A1 and B1 interacts with the carbonyl of aspartic acid D358 in the back of the pocket, respectively through an H-bond and halogen bond. On the other hand, the highest confidence pose of compound C2 highlights a pi-stacking interaction with the gatekeeper residue tyrosine Y288, as well as H-bonds to both Y288 and the catalytic lysine K239. Across the compounds, aliphatic sp³-rich motifs are situated toward the solvent exposed region of the pocket.

The HydraScreen-provided insights into the compound poses and the different interactions of scaffold motifs aids further compound design by highlighting areas and interactions to exploit not only around a specific scaffold, but also from one scaffold to another. The hit compound activity, novelty, and ample positions to tailor, render them attractive scaffolds for further structure-activity relationship (SAR) exploration and subsequent hit-to-lead development.

4 Discussion

Prospective validation of HydraScreen and hit identification in IRAK1

In this study, we propose an augmented drug discovery workflow that relies on Ro5's AI and data science platform while utilizing Stateos' robotic labs capabilities. We show how target evaluation driven by Ro5's SpectraView allowed for the selection of IRAK1 serine-threonine kinase target with emerging therapeutic links to cancers and inflammation. We provide evidence for HydraScreen's virtual screening performance. Notably, Ro5's HydraScreen provides high hit discovery rates in virtual screening, with upwards of 15.9% hits and all of the 3 nanomolar scaffolds ranked in the top 1%. Moreover, HydraScreen's performance increased with stricter thresholds for experimental hit selection - 23.8% hit rate in top 1% of the ranked compounds using greater than 80% relative inhibition of IRAK1 as threshold. All of the distinct nanomolar and high nanomolar scaffolds were ranked in the top 50% of the compounds. HydraScreen is able to prioritize highly active compounds and does not exhibit biases in terms of treatment of structurally diverse compounds. Importantly, HydraScreen has not been trained on IRAK1 data, so these results also reflect on the model's ability to generalize to an unseen target.

HydraScreen was shown to be superior to traditional, industry-standard methods like *Smina* [24] (molecular docking), *DeCAF* [39] (pharmacophore modeling) and a RF model in terms of hit and scaffold discovery rates. HydraScreen offers state-of-the-art performance in line with the most recent AI models available for protein-ligand binding activity prediction [29]. Beyond the high hit rate, HydraScreen uniquely provides ligand pose confidence scores [3] which can be used when considering modifications of the most potent hits in the later hit-to-lead or lead optimization stages of a drug discovery program.

This study successfully identified potent and novel IRAK1 inhibitors. The 5 most potent nanomolar hits represent 3 distinct scaffolds, which are synthetically accessible. One of the identified nanomolar scaffolds exhibits high similarity to a known Pan-RAF inhibitor LY3009120 [15], while the other two are novel when compared to known IRAK1 actives. High molecular weight and lipophilicity were observed for the hits, and will have to be further explored during a medicinal chemistry program. The HydraScreen predicted binding of the hit compounds highlighted the scope to optimize these scaffolds. The highest confidence poses indicated multiple IRAK1-ligand interactions to draw on for SAR exploration, both around a single scaffold and between scaffolds.

The most important contribution of this study is the prospective validation of HydraScreen for virtual screening. Prospective virtual screening evaluation studies

reported in the literature usually experimentally test only a small fraction of the library, well below 1% - a median of 44 compounds based on 401 studies [49]. The median of hit rates reported in these studies is approximately $\sim 11.76\%$ for 385 studies across all target classes and $\sim 9.61\%$ for 67 studies focusing on kinases [49]. However, the reported hit rates are prone to bias due to a small test size. A comparable study that used a support-vector machine model for virtual screening in IRAK1 reported a 2.83% hit rate (1/38) with the most potent compounds reaching $2\mu\text{M}$ activity [7]. In contrast, we screened the entire 47k library to provide a robust assessment of HydraScreen and report a hit discovery rate of upwards of 15.9% for the top 1% (470) of tested compounds, which is well above the median and substantially higher than the comparable IRAK1 virtual screening study [7]. Furthermore, HydraScreen achieves even better hit rates (up to 23.8%, greater than the 3rd quartile 23.5% of hit rates reported in [49]) for higher IRAK1 inhibition thresholds. This is an important observation, since HTS assays are inherently noisy and have their own intrinsic false-positive rates [50]. HydraScreen's evaluation at stricter IRAK1 inhibition thresholds is potentially more representative of its true performance due to a higher confidence in the hits selected from the assay (i.e. lower false-positive rate).

Summary

This study provides compelling evidence for the effectiveness of Ro5's innovative tools, SpectraView and HydraScreen in early stage drug discovery. Using SpectraView target evaluation, we prioritize IRAK1 serine-threonine kinase with emergent therapeutic links in inflammation and cancers. By leveraging Ro5's HydraScreen and Strateos' automated labs, we show how AI-driven virtual screening with HydraScreen could offer high hit discovery rates and reduce experimental costs. In the top 1% of the ranked compounds, HydraScreen identified all three nanomolar classes, and almost a quarter of the total actives in the library at $\geq 80\%$ relative inhibition of IRAK1. The unbiased, prospective evaluation of HydraScreen and comparison against industry-standard methods supports the reliability and robustness of our findings. Ro5's SpectraView and HydraScreen provide innovative methods that can expedite the early stages of drug discovery.

5 Acknowledgements

At Ro5 we are grateful to Tim Kras, Mikhail Demtchenko, and Charles Dazler Knuff for enriching our scientific discussions. Special thanks to Siim Schults and Dainius Salkauskas their pivotal role in the development of our web applications and their indispensable support in translating our research code into reliable drug discovery platforms for deployment to the cloud. At Strateos we acknowledge the contributions of Carsten Andersen and Maxim Ratnikov in terms of experimental design and medicinal chemistry considerations. This study has been funded by Charles Dazler Knuff and Strateos.

References

- [1] Milad Abolhasani and Eugenia Kumacheva. The rise of self-driving labs in chemical and materials sciences. *Nature Synthesis*, 2:483–492, 1 2023.
- [2] Melissa F Adasme, Katja L Linnemann, Sarah Naomi Bolz, Florian Kaiser, Sebastian Salentin, V Joachim Haupt, and Michael Schroeder. PLIP 2021: expanding the scope of the protein–ligand interaction profiler to DNA and RNA. *Nucleic Acids Research*, 49(W1):W530–W534, 05 2021.
- [3] Hisham Abdel Aty Tanya Paquet Gintautas Kamuntavicius Povilas Norvaissas Roy Tal Alvaro Prat, Piero Gasparotto. Hydrascreen: A generalizable structure-based deep learning approach to drug discovery. *ArXiv*, 9 2023.
- [4] Vincent D Blondel, Jean-Loup Guillaume, Renaud Lambiotte, and Etienne Lefebvre. Fast unfolding of communities in large networks. *Journal of Statistical Mechanics: Theory and Experiment*, 2008(10):P10008, oct 2008.
- [5] Denise Carvalho-Silva, Andrea Pierleoni, Miguel Pignatelli, Chuang Kee Ong, Luca Fumis, Nikiforos Karamanis, Miguel Carmona, Adam Faulconbridge, Andrew Hercules, Elaine McAuley, Alfredo Miranda, Gareth Peat, Michaela Spitzer, Jeffrey Barrett, David G. Hulcoop, Eliseo Papa, Gautier Koscielny, and Ian Dunham. Open targets platform: New developments and updates two years on. *Nucleic Acids Research*, 47:D1056–D1065, 1 2019.
- [6] H. C. Stephen Chan, Hanbin Shan, Thamani Dahoun, H. Vogel, and Shuguang Yuan. Advancing drug discovery via artificial intelligence, 8 2019.
- [7] Jinxin Che, Ruiwei Feng, Jian Gao, Hongyun Yu, Qinjie Weng, Qiaojun He, Xiaowu Dong, Jian Wu, and Bo Yang. Evaluation of artificial intelligence in participating structure-based virtual screening for identifying novel interleukin-1 receptor associated kinase-1 inhibitors. *Frontiers in Oncology*, 10, 9 2020.
- [8] Beryl W. Dominy Paul J. Feeney Christopher A. Lipinski, Franco Lombardo. Experimental and computational approaches to estimate solubility and permeability in drug discovery and development settings. *Advanced Drug Delivery Reviews*, 23, 1997.
- [9] Gabriele Corso, Hannes Stärk, Bowen Jing, Regina Barzilay, and Tommi Jaakkola. Diffdock: Diffusion steps, twists, and turns for molecular docking. 10 2022.
- [10] Michael Dickson and Jean Gagnon. The cost of new drug discovery and development. *Discovery medicine*, 4:172–9, 06 2004.

- [11] Schuffenhauer A. Ertl, P. Estimation of synthetic accessibility score of drug-like molecules based on molecular complexity and fragment contributions. *Journal of Cheminformatics*, 8, 2009.
- [12] Cheng Fang, Ye Wang, Richard Grater, Sudarshan Kapadnis, Cheryl Black, Patrick Trapa, and Simone Sciabola. Prospective validation of machine learning algorithms for absorption, distribution, metabolism, and excretion prediction: An industrial perspective. *Journal of Chemical Information and Modeling*, 63(11):3263–3274, 2023. PMID: 37216672.
- [13] Paul G. Francoeur, Tomohide Masuda, Jocelyn Sunseri, Andrew Jia, Richard B. Iovanisci, Ian Snyder, and David R. Koes. Three-dimensional convolutional neural networks and a crossdocked data set for structure-based drug design. *Journal of Chemical Information and Modeling*, 60:4200–4215, 9 2020.
- [14] John M. Hatcher, Guang Yang, Li Wang, Scott B. Ficarro, Sara Buhrlage, Hao Wu, Jarrod A. Marto, Steven P. Treon, and Nathanael S. Gray. Discovery of a selective, covalent irak1 inhibitor with antiproliferative activity in myd88 mutated b-cell lymphoma. *ACS Medicinal Chemistry Letters*, 11:2238–2243, 11 2020.
- [15] James R. Henry, Michael D. Kaufman, Sheng-Bin Peng, Yu Mi Ahn, Timothy M. Caldwell, Lakshminarayana Vogeti, Hanumaiah Telikepalli, Weiping Lu, Molly M. Hood, Thomas J. Rutkoski, Bryan D. Smith, Subha Vogeti, David Miller, Scott C. Wise, Lawrence Chun, Xiaoyi Zhang, Youyan Zhang, Lisa Kays, Philip A. Hipskind, Aaron D. Wroblewski, Karen L. Lobb, Julia M. Clay, Jeffrey D. Cohen, Jennie L. Walgren, Denis McCann, Phenil Patel, David K. Clawson, Sherry Guo, Danalyn Manglicmot, Chris Groshong, Cheyenne Logan, James J. Starling, and Daniel L. Flynn. Discovery of 1-(3,3-dimethylbutyl)-3-(2-fluoro-4-methyl-5-(7-methyl-2-(methylamino)pyrido[2,3-d]pyrimidin-6-yl)phenyl)urea (ly3009120) as a pan-raf inhibitor with minimal paradoxical activation and activity against braf or ras mutant tumor cells. *Journal of Medicinal Chemistry*, 58:4165–4179, 2015.
- [16] Ian Holland and Jamie A. Davies. Automation in the life science research laboratory, 11 2020.
- [17] Mona M. Hosseini, Stephen E. Kurtz, Sherif Abdelhamed, Shawn Mahmood, Monika A. Davare, Andy Kaempf, Johannes Elferich, Jason E. McDermott, Tao Liu, Samuel H. Payne, Ujwal Shinde, Karin D. Rodland, Motomi Mori, Brian J. Druker, Jack W. Singer, and Anupriya Agarwal. Inhibition of interleukin-1 receptor-associated kinase-1 is a therapeutic strategy for acute myeloid leukemia subtypes. *Leukemia*, 32:2374–2387, 11 2018.
- [18] Muhammad Jahangir Hossen, Woo Seok Yang, Daewon Kim, Adithan Aravinthan, Jong Hoon Kim, and Jae Youl Cho. Thymoquinone: An irak1 inhibitor with in vivo and in vitro anti-inflammatory activities. *Scientific Reports*, 7, 2 2017.
- [19] J. P. Hughes, S. S. Rees, S. B. Kalindjian, and K. L. Philpott. Principles of early drug discovery, 3 2011.
- [20] Fergus Imrie, Anthony R Bradley, and Charlotte M Deane. Generating property-matched decoy molecules using deep learning. *Bioinformatics*, 02 2021.

- [21] José Jiménez, Miha Škalič, Gerard Martínez-Rosell, and Gianni De Fabritiis. Kdeep: Protein-ligand absolute binding affinity prediction via 3d-convolutional neural networks. *Journal of Chemical Information and Modeling*, 58:287–296, 2 2018.
- [22] Sunghwan Kim, Jie Chen, Tiejun Cheng, Asta Gindulyte, Jia He, Siqian He, Qingliang Li, Benjamin A. Shoemaker, Paul A. Thiessen, Bo Yu, Leonid Zaslavsky, Jian Zhang, and Evan E. Bolton. Pubchem 2019 update: Improved access to chemical data. *Nucleic Acids Research*, 47:D1102–D1109, 1 2019.
- [23] Jonathan Knowles and Gianni Gromo. Target selection in drug discovery, 1 2003.
- [24] David Ryan Koes, Matthew P. Baumgartner, and Carlos J. Camacho. Lessons learned in empirical scoring with smina from the csar 2011 benchmarking exercise. *Journal of Chemical Information and Modeling*, 53:1893–1904, 8 2013.
- [25] Andrei Kouranov, Lei Xie, Joanna de la Cruz, L. Chen, John Westbrook, Philip E. Bourne, and Helen M. Berman. The rcsb pdb information portal for structural genomics. *Nucleic acids research*, 34, 2006.
- [26] C Lamagna, M Chan, E Tai, S Siu, R Frances, S Yi, C Young, V Markovtsov, Y Chen, L Chou, G Park, E Masuda, and V Taylor. Op0133 preclinical efficacy of r835, a novel irak1/4 dual inhibitor, in rodent models of joint inflammation. *Annals of the Rheumatic Diseases*, 79:86, 2020.
- [27] Eduardo Habib Bechelane Maia, Letícia Cristina Assis, Tiago Alves de Oliveira, Alisson Marques da Silva, and Alex Gutterres Taranto. Structure-based virtual screening: From classical to artificial intelligence, 4 2020.
- [28] Andrew T. McNutt, Paul Francoeur, Rishal Aggarwal, Tomohide Masuda, Rocco Meli, Matthew Ragoza, Jocelyn Sunseri, and David Ryan Koes. Gnina 1.0: molecular docking with deep learning. *Journal of Cheminformatics*, 13, 12 2021.
- [29] Rocco Meli, Garrett M. Morris, and Philip C. Biggin. Scoring functions for protein-ligand binding affinity prediction using structure-based deep learning: A review. *Frontiers in Bioinformatics*, 2, 6 2022.
- [30] N. Arul Murugan, Gnana Ruba Priya, G. Narahari Sastry, and Stefano Markidis. Artificial intelligence in virtual screening: Models versus experiments, 7 2022.
- [31] Daniel Probst and Jean Louis Reymond. A probabilistic molecular fingerprint for big data settings. *Journal of Cheminformatics*, 10, 12 2018.
- [32] Michael G. Rolf, Jon O. Curwen, Margaret Veldman-Jones, Cath Eberlein, Jianyan Wang, Alex Harmer, Caroline J. Hellowell, and Martin Braddock. In vitro pharmacological profiling of r406 identifies molecular targets underlying the clinical effects of fostamatinib. *Pharmacology Research and Perspectives*, 3, 10 2015.
- [33] Semion K. Saikin, Christoph Kreisbeck, Dennis Sheberla, Jill S. Becker, and A. Aspuru-Guzik. Closed-loop discovery platform integration is needed for artificial intelligence to make an impact in drug discovery, 1 2019.
- [34] Gisbert Schneider. Automating drug discovery. *Nature Reviews Drug Discovery*, 17:97–113, 2018.
- [35] Petra Schneider, W. Patrick Walters, Alleyn T. Plowright, Norman Sieroka, Jennifer Listgarten, Robert A. Goodnow, Jasmin Fisher, Johanna M. Jansen, José S.

- Duca, Thomas S. Rush, Matthias Zentgraf, John Edward Hill, Elizabeth Krutohollow, Matthias Kohler, Jeff Blaney, Kimito Funatsu, Chris Luebkeemann, and Gisbert Schneider. Rethinking drug design in the artificial intelligence era, 5 2020.
- [36] Adrian M. Schreyer and Tom Blundell. Usrnat: Real-time ultrafast shape recognition with pharmacophoric constraints. *Journal of Cheminformatics*, 4, 11 2012.
- [37] Maxim V. Shapovalov and Roland L. Dunbrack. A smoothed backbone-dependent rotamer library for proteins derived from adaptive kernel density estimates and regressions. *Structure*, 19:844–858, 6 2011.
- [38] Valentin Steinwandter, Daniel Borchert, and Christoph Herwig. Data science tools and applications on the way to pharma 4.0, 9 2019.
- [39] Marta M. Stepniewska-Dziubinska, Piotr Zielenkiewicz, and Pawel Siedlecki. Decaf-discrimination, comparison, alignment tool for 2d pharmacophores. *Molecules (Basel, Switzerland)*, 22, 7 2017.
- [40] Jocelyn Sunseri and David Ryan Koes. Pharmit: interactive exploration of chemical space. *Nucleic Acids Research*, 44:W442–W448, 7 2016.
- [41] Oliver T. Unke, Stefan Chmiela, Huziel E. Saucedo, Michael Gastegger, Igor Poltavsky, Kristof T. Schütt, Alexandre Tkatchenko, and Klaus Robert Müller. Machine learning force fields, 8 2021.
- [42] Jessica Vamathevan, Dominic Clark, Paul Czodrowski, Ian Dunham, Edgardo Ferran, George Lee, Bin Li, Anant Madabhushi, Parantu Shah, Michaela Spitzer, and Shanrong Zhao. Applications of machine learning in drug discovery and development, 6 2019.
- [43] Li Wang, Qi Qiao, Ryan Ferrao, Chen Shen, John M. Hatcher, Sara J. Buhrlage, Nathanael S. Gray, and Hao Wu. Crystal structure of human irak1. *Proceedings of the National Academy of Sciences of the United States of America*, 114:13507–13512, 12 2017.
- [44] Zhen Ning Wee, Siti Maryam J.M. Yatim, Vera K. Kohlbauer, Min Feng, Jian Yuan Goh, Bao Yi, Puay Leng Lee, Songjing Zhang, Pan Pan Wang, Elgene Lim, Wai Leong Tam, Yu Cai, Henrik J. Ditzel, Dave S.B. Hoon, Ern Yu Tan, and Qiang Yu. Irak1 is a therapeutic target that drives breast cancer metastasis and resistance to paclitaxel. *Nature Communications*, 6, 10 2015.
- [45] Scott A. Wildman and Gordon M. Crippen. Prediction of physicochemical parameters by atomic contributions. *Journal of Chemical Information and Computer Sciences*, 39, 1999.
- [46] David S. Wishart, Yannick D. Feunang, An C. Guo, Elvis J. Lo, Ana Marcu, Jason R. Grant, Tanvir Sajed, Daniel Johnson, Carin Li, Zinat Sayeeda, Nazanin Assempour, Ithayavani Iynkkaran, Yifeng Liu, Adam MacIejewski, Nicola Gale, Alex Wilson, Lucy Chin, Ryan Cummings, DIana Le, Allison Pon, Craig Knox, and Michael Wilson. Drugbank 5.0: A major update to the drugbank database for 2018. *Nucleic Acids Research*, 46:D1074–D1082, 1 2018.
- [47] Xiangxiang Zeng, Xinqi Tu, Yuansheng Liu, Xiangzheng Fu, and Yansen Su. Toward better drug discovery with knowledge graph, 2 2022.
- [48] Hao Zhu. Big data and artificial intelligence modeling for drug discovery. *Annual Review of Pharmacology and Toxicology*, 2019.

- [49] Hui Zhu, Yulin Zhang, Wei Li, and Niu Huang. A comprehensive survey of prospective structure-based virtual screening for early drug discovery in the past fifteen years, 12 2022.
- [50] Tian Zhu, Shuyi Cao, Pin Chih Su, Ram Patel, Darshan Shah, Heta B. Chokshi, Richard Szukala, Michael E. Johnson, and Kirk E. Hevener. Hit identification and optimization in virtual screening: Practical recommendations based on a critical literature analysis, 9 2013.

Appendix A SpectraView

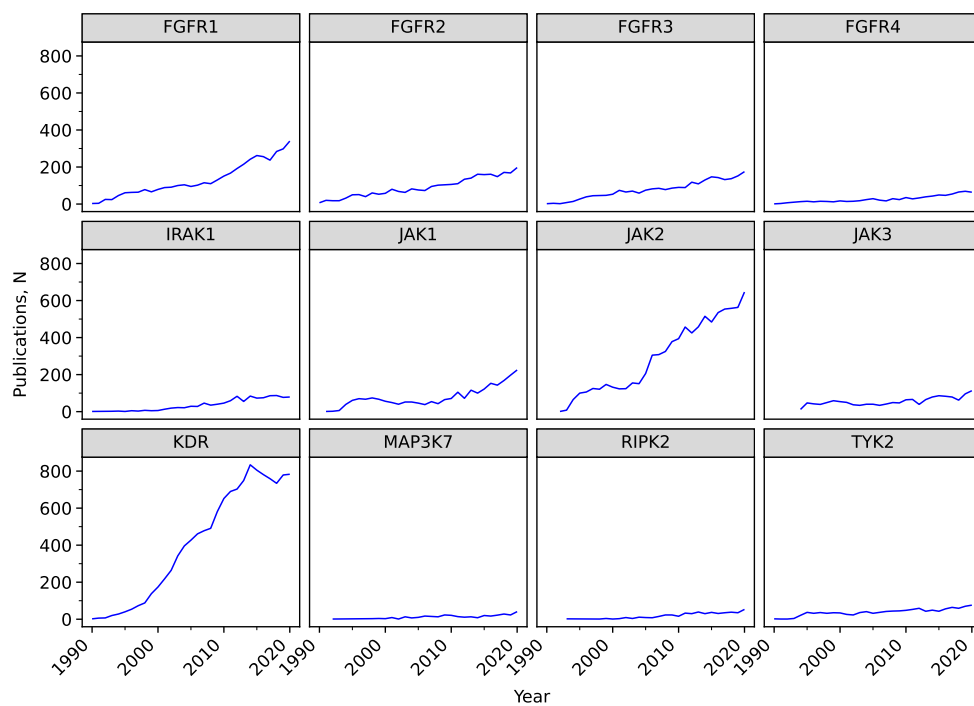


Fig. A1: PubMed-indexed publication trends over the last 3 decades for each of the considered targets.

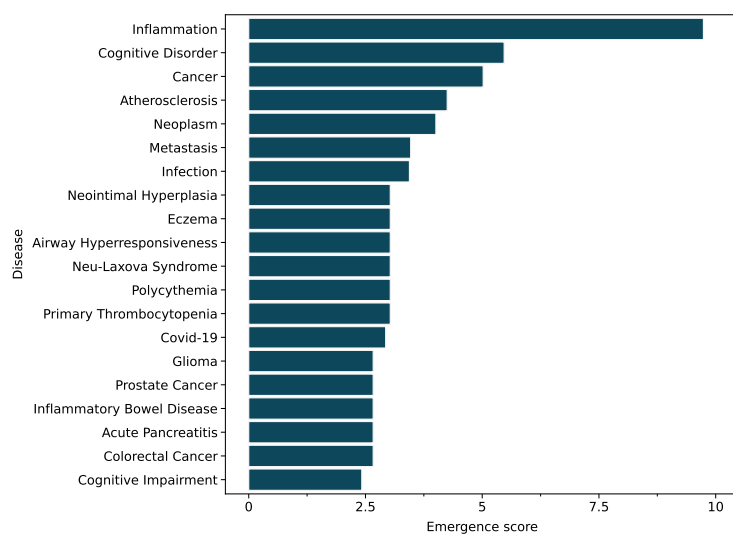


Fig. A2: Emergence scores (ES) for different diseases linked to IRAK1. The emergence score is calculated as a maximum increase in the number of publications per disease scaled by the total publication volume and recency.

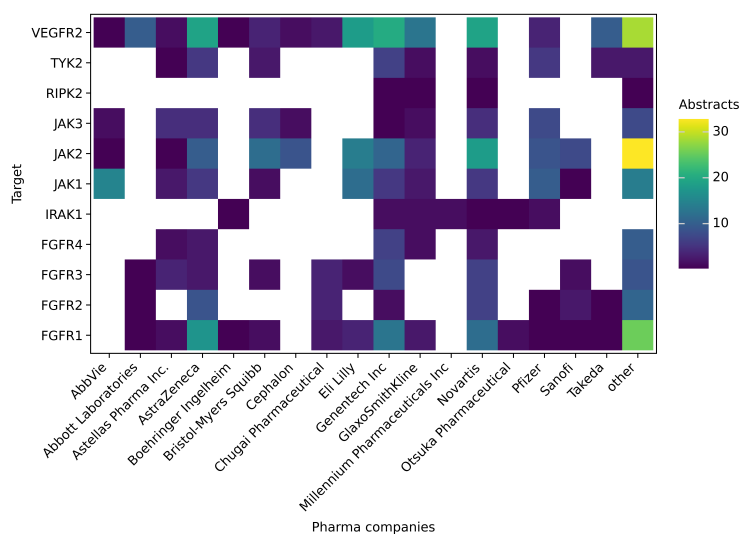


Fig. A3: Total number of PubMed-indexed publications with pharma company affiliations that at least one of the considered targets.

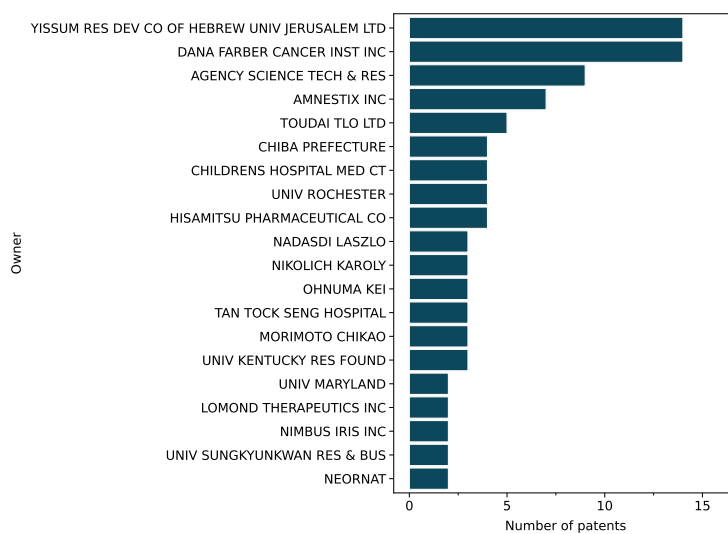


Fig. A4: Organizations that own the most patents or patent applications that mention IRAK1.

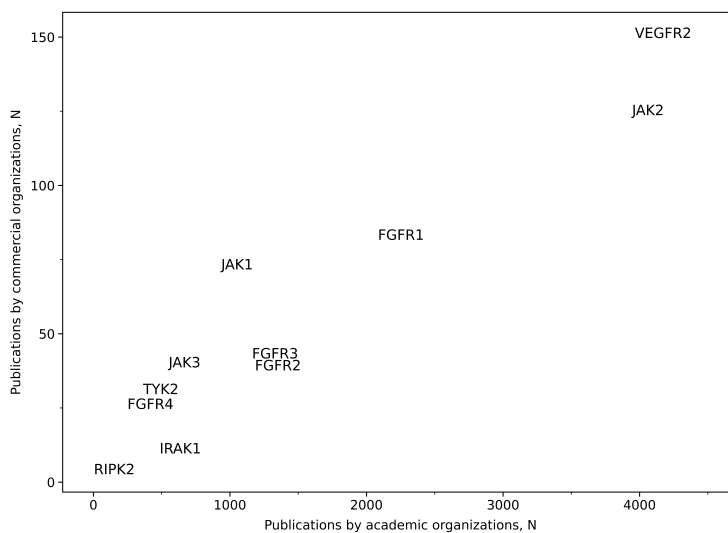


Fig. A5: The correlation between the number of PubMed-indexed publications affiliated with academic or pharma organizations for each of the considered targets.